

Distributed Control of HVAC-BESS under Solar Power Forecasts in Microgrid System

Abstract—This paper investigates an energy management problem in the microgrid by scheduling heating ventilation air conditioning (HVAC) and battery energy storage system (BESS) with a distributed algorithm. A multi-layer energy management architecture is presented at a system-level to co-optimize the HVAC-BESS by taking into account solar energy forecasts. A surplus-based consensus algorithm is proposed to solve the optimization problem, where the local power mismatch is introduced as a surplus term, and the HVAC-BESS can thus be co-scheduled to maximize renewable energy efficiency at the peak generation time. A set of the convex cost functions are formulated to minimize the HVAC’s user dissatisfaction degree and alleviate power loss during the BESS operation. The goal is to collectively minimize the total energy cost in a distributed manner, subject to individual load constraints and power balance constraints. It is theoretically proved that a global convergence of the proposed algorithm is achieved provided that the directed network is strongly connected. The results from a number of case studies are promising, demonstrating the effectiveness and robustness of the algorithm under practical scenarios.

Index Terms—Energy management system, HVAC, BESS, multi-layer energy management, surplus-based consensus algorithm, directed network.

I. INTRODUCTION

WITH the growth of renewable energy sources, microgrids have employed energy management scheme to flatten power fluctuations and alleviate power imbalance resulted from weather uncertainties. Hence, according to the solar power forecasts, dynamic controlling of the load demand through an intelligent management solution can promote the prosperity of green energy technology. The battery energy storage system (BESS) has become an unequivocal choice to shift the load from the off-peak to peak generation time and reduce the energy cost [1]. It is reported that heating, ventilation and air conditioning (HVAC) systems consume approximately half of the energy used by buildings [2]. The thermal mass in a building can be regarded as a virtual energy storage system to store thermal energy by preheating/precooling the rooms at peak generation times and reduce power consumption at peak load times [1]. This creative idea can be extended to other thermal appliances, such as the electrical and water heaters. Therefore,

BESS and HVAC can work as the energy buffer to enhance stability and robustness of the microgrids.

Challenges faced within the control and optimization of BESS or HVACs have been addressed widely in [3]–[8]. The authors in [3] improved the energy efficiency of the HVAC by using a learning-based model predictive control (MPC) to maintain the room temperature within a comfortable level. The experimental result showed that energy consumption was reduced by 30%–70%. In [4], the authors utilized the MPC to control HVACs to save energy bills and improve power balance. Likewise, the authors in [5] and [6] proposed centralized energy management solutions to regulate demand response and develop pricing strategy for consumers by controlling HVAC systems. However, these approaches are essentially centralized schemes, which require high computation capacity and wider communication bandwidth. In order to overcome these technical barriers, the authors in [9] investigated a distributed consensus algorithm to address the active power imbalance issue in the microgrid by regulating compressor frequency for the distributed HVACs. In the meantime, centralized and distributed approaches have also been widely used in aggregated BESSs to provide an ancillary service for the utility, as demonstrated in [10]–[12]. The authors in [10] focused on a power-sharing algorithm to optimize the energy efficiency for multiple BESSs, by taking into account power boundary constraints. In [11], the authors considered different characteristics of BESSs and incorporated a consensus control strategy into the heterogeneous BESSs. Furthermore, the author in [13] proposed a novel cooperative distributed algorithm for charging the electrical vehicles, where the system

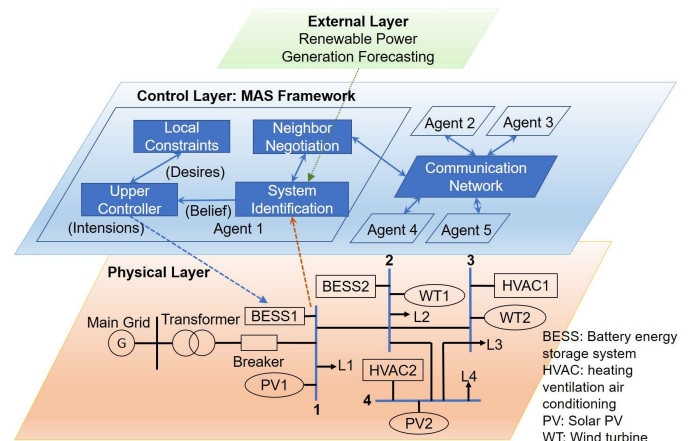


Fig 1. A multi-layer energy management architecture

gain robustness against node failures. However, it is worth noting that, although effective, the above approaches have considered either HVAC or BESS alone and the combined HVAC-BESS effects were not yet studied.

Combined HVAC and battery have also been scheduled to develop an efficient building energy management system [1], [14], [15]. In [1], batteries and HVACs were co-optimized with MPC to reduce the total energy cost and maintain the user's comfort level. The authors in [15] proposed a system-level approach to co-schedule the control of BESS and HVAC and developed a battery management system tailored to the building testbed. However, these approaches were developed from perspective of the individual users to achieve their financial and comfort benefits by means of independent management, whilst neglecting contributions to the utility. In [14], the authors proposed a two-stage strategy to study the usage of BESS and HVAC for frequency regulation and energy cost minimization. This centralized approach, however, was too challenging to accommodate a large-scale power grid or a distributed power network. In this paper, we will address the problem from both the individual level to maximize user comfortability in terms of energy use and improve charging efficiency for HVAC and BESS respectively by developing an energy dispatch scheme at the system level to alleviate the power imbalance at peak load/generation times by employing a distributed control scheme.

This paper proposes a distributed energy management approach for the microgrid by considering hybrid HVAC-BESS units and incorporating solar power forecasts. It is noted here that to ensure consistency of the load units, only the charging mode of BESS is taken into account in the paper, i.e., the BESS is considered as a load and operates in the charging mode. Fig 1 shows a hierarchical architecture of the proposed framework. The external layer forecasts the local renewable power generation (solar power forecasting in our study). The control layer performs a surplus-based distributed algorithm under a multi-agent system (MAS) framework and provides the power reference to HVACs and BESSs based on the forecasting results. The physical layer is responsible for monitoring and regulating the lower controller at HVAC and BESS units to track the desired power reference. The block functionality and information flows in Fig. 1 will be explained in the Section III. A surplus-based consensus algorithm is designed to solve the resource allocation problem by computing optimal power references for HVACs and BESSs, in response to the local power mismatch and power sharing information with their neighbours. It is proved that if the directed communication network among the units is strongly connected, the behaviour of the system converges to the global optimum. This would minimize the power loss of battery charging, maximize the satisfaction degree of HVAC users and alleviate the power imbalance caused by the intermittent renewable energy.

The main contributions of the paper are summarized in threefold aspects.

1) BESS and HVAC are jointly studied through a distributed approach to enhance the active power balance in the microgrid, which expands the application in [16]. It helps

improve energy storage capacity, avoid installation of additional storage devices and save energy storage costs.

- 2) The designed surplus-based consensus algorithm enables to solve distributed control problem under directed communication network, whereas the most literatures have focused on distributed problem under undirected graph. Our consensus algorithm helps to relax topology conditions in [17]. A number of case studies are conducted to demonstrate its dynamics, robustness, and scalability.
- 3) A short-term solar power forecast by means of real data is performed to estimate the energy uncertainties, in order to develop appropriate demand response programs. The existing researches, e.g., [18], [19], have not considered renewable energy forecast and its intermittency effects.

The remainder of this paper is organized as follows. Section II presents preliminaries and problem formulations. Section III introduces the surplus-based consensus algorithm for problem optimization and provides algorithm implementation in detail. The main results are examined through extensive case studies in Section IV, followed by the conclusion in Section V.

II. PRELIMINARIES AND PROBLEM FORMULATION

A. Graph theory

A microgrid is usually regarded as a MAS, where the HVAC and BESS act as agents. The agents and communication between agents are considered as nodes and edges respectively to construct a directed graph. Let define a directed graph $\mathcal{G} = (\mathcal{V}, \mathcal{E})$, which is composed of a nonempty finite set of nodes $\mathcal{V} = \{1, 2, \dots, n\}$ and a finite set of edges $\mathcal{E} = \{(i, j) | i, j \in \mathcal{V}\} \subset \mathcal{V} \times \mathcal{V}$. The information transmitted from nodes i to j is denoted as an edge (j, i) . If any node in a directed graph can find a communication path to any other nodes, this digraph is said to be strongly connected.

For any node i in \mathcal{V} , its in-neighbour set and out-neighbour set are denoted by $\mathcal{N}_i^+ = \{j | (j, i) \in \mathcal{E}\}$ and $\mathcal{N}_i^- = \{j | (i, j) \in \mathcal{E}\}$, respectively. Correspondingly, its in-degree and out-degree of node i are denoted by $d_i^+ = |\mathcal{N}_i^+|$ and $d_i^- = |\mathcal{N}_i^-|$, respectively, where $|\cdot|$ represents the cardinality of a set. For a strongly connected digraph, assume that there are no self-loop edges and repeated edges, the communication network can be defined mathematically by matrices P and Q with p_{ij} and q_{ij} as the ij th element, such that:

$$p_{ij} = \begin{cases} \frac{1}{1 + d_i^+} & j \in \mathcal{N}_i^+ \\ 1 - \frac{1}{1 + d_i^+} & i = j \\ 0 & j \notin \mathcal{N}_i^+ \end{cases} \quad q_{ij} = \begin{cases} \frac{1}{1 + d_i^-} & j \in \mathcal{N}_i^- \\ 1 - \frac{1}{1 + d_i^-} & i = j \\ 0 & j \notin \mathcal{N}_i^- \end{cases} \quad (1)$$

It can be seen that P and Q are nonnegative matrix for a strongly connected graph, where in P every row sums up to one and in Q each column sums up to one [18].

B. Problem formulations

Each HVAC or BESS aims to maximize its benefits when playing a role in maintaining the network power balance. Therefore, the objective functions for HVAC and BESS are

given, respectively, as follows.

1) Comfort maximization for HVAC users

The first objective of the proposed strategy is to maximize the comfort level for HVAC users. A utility function ($U_{AC,i}$) is used to indicate the satisfaction level in comfortability for HVAC users. Generally, $U_{AC,i}$ represents a function of power consumption $P_{AC,i}$ for the i th HVAC. A general form of the utility function can be expressed as [20]:

$$U_{AC,i}(P_{AC,i}) = \begin{cases} \omega_i P_{AC,i} - \alpha_i P_{AC,i}^2, & P_{AC,i} < \frac{\omega_i}{2\alpha_i} \\ \frac{\omega_i^2}{4\alpha_i}, & P_{AC,i} \geq \frac{\omega_i}{2\alpha_i} \end{cases} \quad (2)$$

where ω_i and α_i are coefficients indicating the comfort sensitivity of different users. $U_{AC,i}$ is chosen as a concave function with a value of zero at $P_{AC,i} = 0$. The utility function (2) has the following features:

- It is a non-decreasing function, i.e., the first-order differential of $U_{AC,i}$ with respect to $P_{AC,i}$ is non-negative.
- The satisfaction degree becomes saturated with excessive power consumption, i.e., the second-order differential of $U_{AC,i}$ with respect to $P_{AC,i}$ is also non-positive.

It is noted that $U_{AC,i}$ in the HVAC model in this paper represents essentially a comfortability cost measuring the user comfortability in terms of power consumption and thus energy cost from the HVACs, rather than temperature.

2) Charging power maximization of BESS

The second objective is to minimize the charging power loss of BESS due to its internal resistance. The change in energy level of the i th BESS can be expressed as [21]:

$$\Delta E(t) = P_{B,i} \eta_i(P_{B,i}) \quad (3)$$

where charging power $P_{B,i} > 0$, as we assumed that the BESSs only operate in charging mode. η_i is charging efficiency which reflects how much energy is fully stored and can be modelled with consideration of power loss of battery [16], [21]:

$$\eta_i = a_i - b_i P_{B,i} \quad (4)$$

where a_i and b_i are charging parameters related to battery i . By substituting (4) into (3), a quadratic relationship between $P_{B,i}$ and $\Delta E(t)$ is derived.

$$C_{B,i}(P_{B,i}) = \Delta E = (a_i - b_i P_{B,i}) P_{B,i} \quad (5)$$

where the $C_{B,i}$ denotes the objective function of BESS. In order to operate the microgrid in an economical way, eq (5) should aim to maximally increase the energy level of battery by adjusting $P_{B,i}$.

C. Problem optimization

By combing (2) and (5), the objective of multiple HVACs and BESSs is to maximize the following function.

$$\max \sum_{i \in S_{AC}} U_{AC,i}(P_{AC,i}) + \sum_{i \in S_B} C_{B,i}(P_{B,i}) \quad (6)$$

$$\text{s.t.} \quad \sum_{i \in S_{AC}} P_{AC,i} + \sum_{i \in S_B} P_{B,i} = P_d \quad (7)$$

$$\underline{P}_{AC,i} \leq P_{AC,i} \leq \bar{P}_{AC,i} \quad \underline{P}_{B,i} \leq P_{B,i} \leq \bar{P}_{B,i} \quad (8)$$

where $\underline{P}_{AC,i}$, $\bar{P}_{AC,i}$, $\underline{P}_{B,i}$ and $\bar{P}_{B,i}$ are lower and upper power limit for the HVAC and BESS, respectively. P_d represents the

total power mismatch. S_{AC} and S_B represent sets of the HVAC and BESS units, respectively. The objective function (6) is proposed to jointly solve the optimization goal of both HVAC and BESS. Once (6) is achieved, the sub-optimization problems for HVAC and BESS can be achieved, respectively.

For convenience, P_i represents power consumption of HVACs and BESSs at node i , as denoted by $P_i = \{P_{AC,i}, P_{B,i}\}$.

The problems (6)-(8) can be rewritten as:

$$\min \sum_{i \in S_{AC} \cup S_B} F_i(P_i) \quad (9)$$

$$\text{s.t.} \quad \sum_{i \in S_{AC} \cup S_B} P_i = P_d \quad (10)$$

$$\underline{P}_i \leq P_i \leq \bar{P}_i, \text{ for } \forall i \in S_{AC} \cup S_B \quad (11)$$

where $F_i(P_i) = -U_{AC,i}(P_{AC,i}) - C_{B,i}(P_{B,i})$, \underline{P}_i and \bar{P}_i indicate the power boundaries of overall HVAC and BESS, as denoted by $\underline{P}_i = \{\underline{P}_{AC,i}, \underline{P}_{B,i}\}$ and $\bar{P}_i = \{\bar{P}_{AC,i}, \bar{P}_{B,i}\}$. $F_i(P_i)$ is a convex function for the i th node, satisfying the following conditions:

Assumption 1: $F_i(P_i)$ is second-order differentiable in \mathbb{R} and its second derivative value is bounded with respect to $[\underline{P}_i, \bar{P}_i]$.

$$\frac{\partial^2 F_i(P_i)}{\partial P_i^2} \geq \ell_i \geq 0, \forall \underline{P}_i \leq P_i \leq \bar{P}_i \quad (12)$$

where ℓ_i is a constant coefficient regarding node i .

Remark: Due to the local power limit of HVACs and BESSs, the global power mismatch should be within the maximum power range, such that:

$$\sum_{i \in S_{AC} \cup S_B} \underline{P}_i \leq P_d \leq \sum_{i \in S_{AC} \cup S_B} \bar{P}_i \quad (13)$$

With regards to the objective function (9), we define an incremental cost function as below:

$$J_i(P_i) = \frac{dF_i(P_i)}{dP_i} \quad (14)$$

Since the optimization problem (9)-(11) is a convex optimization problem with affine constraints, therefore, the Lagrange function L with respect to optimization problem (9)-(11) is formulated as:

$$L(P_i, \lambda) = \sum_{i=1}^n F_i(P_i) + \lambda \left(P_d - \sum_{i=1}^n P_i \right) \quad (15)$$

where λ is Lagrange multiplier for equality constraint and $n = \text{card}(S_{AC} \cup S_B)$. Now, we present the optimality condition for problem (9)-(11), which is obtained by Lagrange equivalence.

By [22], P_i^* is the optimal solution to the problem (9)-(11) with λ^* being the optimal Lagrange multiplier of (15) if and only if

$$\begin{cases} J_i(P_i^*) = \lambda^*, \underline{P}_i \leq P_i^* \leq \bar{P}_i \\ J_i(P_i^*) \leq \lambda^*, P_i^* = \bar{P}_i \\ J_i(P_i^*) \geq \lambda^*, P_i^* = \underline{P}_i \end{cases} \quad (16)$$

This indicates the multiplier can be denoted by the incremental cost. The equations (16) can be rewritten as the following form:

$$P_i^* = \Phi_i(\lambda^*) = \begin{cases} J_i^{-1}(\lambda^*), & \text{if } J_i(\underline{P}_i) \leq \lambda^* \leq J_i(\bar{P}_i) \\ \bar{P}_i, & \text{if } \lambda^* > J_i(\bar{P}_i) \\ \underline{P}_i, & \text{if } \lambda^* < J_i(\underline{P}_i) \end{cases} \quad (17)$$

where $\Phi_i(\lambda)$ is a nonlinear projection map of power

consumption P_i regarding the Lagrange multiplier λ . $J_i^{-1}(\lambda^*)$ is the inverse function of $J_i(P_i^*)$. The (17) implies that if the optimal Lagrange multiplier λ^* is obtained, then the global optimal power point P_i^* can be achieved in a distributed manner.

Considering the power constraints on loads, let define Γ_{P_i} as a subset of HVACs and BESSs where the power outputs are saturated. By summing (17) to satisfy (10) while considering (2) and (5), the optimal multiplier λ^* is calculated as:

$$\lambda^* = \frac{P_d - \sum_{i \in \Gamma_{P_i}} P_i - \sum_{i \notin \Gamma_{P_i}} \frac{\gamma_i}{2\beta_i}}{\sum_{i \notin \Gamma_{P_i}} \frac{1}{2\beta_i}} \quad (18)$$

where β_i is a mathematical set of parameters $\{\alpha_i, a_i\}$ and γ_i is a mathematical set of parameters $\{\omega_i, b_i\}$, as derived from (2) and (5).

III. DISTRIBUTED ALGORITHM UNDER SOLAR POWER FORECASTS

In this section, a surplus-based consensus algorithm is presented, allowing each agent to have their own Lagrange multiplier $\lambda_i \in \mathbb{R}^n$ and update λ_i such that all λ_i from the consensus algorithm converge to λ^* , by exchanging information with its neighbours. Moreover, each agent calculates its estimate P_i about the optimal power consumption P_i^* based on the projection map (17), which confines the estimate P_i in the range of $[P_i, \bar{P}_i]$. In order to achieve these, a surplus state $\xi_i \in \mathbb{R}^n$ is introduced to store the local bias between demand and power generation at local bus i at each iteration k . ξ_i is averaged with its neighbours and asymptotically converges to zero.

A. Surplus-based consensus algorithm

The algorithm is shown in Algorithm 1.

Algorithm 1: Surplus-based consensus algorithm

Initialization:

Set $\lambda_i(0), P_i(0), \xi_i(0) \forall i = 1, 2, \dots, n$ as below:

$$\lambda_i(0) = J_i(P_i(0))$$

$$P_i(0) \in [P_i, \bar{P}_i]$$

$$\xi_i(0) = 0$$

Give that a small feedback gain ϵ_i satisfies $\varrho_e \leq \epsilon_i \leq 2\beta_i$ (ϱ_e is defined later in the context).

Iteration:

1. Update λ_i according to

$$\lambda_i(k+1) = \lambda_i(k) + c_i(k) \sum_{j \in \mathcal{N}_i^+} p_{ij} (\lambda_j(k) - \lambda_i(k)) + \epsilon_i \xi_i(k) \quad (19)$$

2. Update P_i , according to

$$P_i(k+1) = \Phi_i(\lambda_i(k+1)) \quad (20)$$

3. Update ξ_i , according to

$$\xi_i(k+1) = q_i \xi_i(k) + \sum_{j \in \mathcal{N}_i^+} q_{ji} \xi_j(k) - (P_i(k+1) - P_i(k)) \quad (21)$$

Output: $\lambda_i(k), P_i(k), \xi_i(k)$ for $\forall i = 1, 2, \dots, n$

The (20) is a general form of (17). The parameters $p_{ij}, q_i, q_{ij}, \epsilon_i$, and $c_i(k)$ satisfy the following properties, for all $i, j = 1, 2, \dots, n$ and every iteration k .

(P1) The connectivity weight updates q_{ij}, p_{ij}, q_i are obtained by (1), where $q_i = q_{ii}$. Note that $\varrho_q \leq q_i \leq 1$, where $\varrho_q = \min_{i=1,2,\dots,n} \{q_i\}$ is a positive constant.

(P2) The feedback gain ϵ_i specifies the amount of power surplus used for incremental cost update and $\epsilon_i = q_i \theta_i$, where $\theta_i \in (0, 2\beta_i)$. ϵ_i is bounded with $[\varrho_e, 2\beta_i]$, where $\varrho_e = \min_{i=1,2,\dots,n} \{\epsilon_i\}$ and $\varrho_e > 0$. ϵ_i has a great effect on the model stability and convergence speed, and more details are demonstrated in the case studies.

(P3) $c_i(k)$ is a switching coefficient. Each agent (node) is allowed to make a positive power surplus based on neighbour's state, such that if $\sum_{j \in \mathcal{N}_i} p_{ij} (\lambda_j(k) - \lambda_i(k)) \leq 0$, $c_i(k) = 1$, otherwise $c_i(k) = 0$.

Theorem 1: The algorithms (19)-(21) converge to the optimal solution to resource allocation problem (9)-(11) if the directed graph is strongly connected.

The complete proof is made based on Lyapunov stability theory, where the non-negative properties of ξ_i and non-decreasing property of minimal λ_i are proved, respectively. The proof details can be seen in Appendix.

Remark: The distributed control scheme is designed based on the consensus algorithm to estimate the global power mismatch via information exchange with neighbours. Thus, this scheme has advantages in reducing communication cost and accelerating control efficiency, as compared with the centralized counterpart.

B. Solar power forecast

As shown in Fig. 1, the external layer is to provide short-term 24-h solar power forecasts. Generally, the forecasting time horizon can be classified into the short-term (half an hour to 6 hours), medium-term (6 hours - 1 day), long-term (1 day - 1 week). Short-term forecasting is used for scheduling and controlling energy flow among power sources, loads and storage devices. Medium-term and long-term forecasting are responsible for price settlement, load dispatch and maintenance scheduling, respectively. The widely used forecasting methods

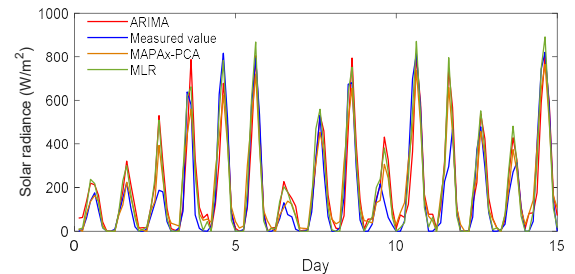


Fig 2. Solar irradiance forecast performance under different models.

TABLE I
THE COMPARISON OF FORECASTING PERFORMANCE

	MLR	ARIMA	MAPAN-PCA
MAE (W/m^2)	67.02	66.69	64.01
RMSE (W/m^2)	98.831	98.193	89.79
NRMSE	0.40	0.41	0.38
R ²	0.83	0.8325	0.85

include machine learning algorithms or statistical techniques [23]–[25]. Here, we used three forecasting techniques, namely, the multiple linear regression (MLR), autoregressive integrated moving average (ARIMA), and a hybrid method of multiple aggregation prediction algorithm (MAPA) and principal components analysis (PCA). The solar irradiance is predicted from a local region in the UK, where datasets are available from two sources. Firstly, a set of weather forecasting indexes are provided by UK Met office via its weather forecast website, where dataset is updated every 3 hours for the next 5 days. Therefore, the dataset at the local weather forecast site is collected. It is known from [26] that the highly related meteorological components selected to predict solar irradiance are ultraviolet index, air temperature and weather type. Secondly, solar irradiance data acquired at the local weather station are also used. The seasonality and lag effect of the time-series data are characterized by dummy variables and lag variables, which are employed to strengthen the accuracy of the forecast model. These two datasets are 3 month long, spanning from April to July 2017, where the first two and half months’ data are employed for model training while the last half-month data are used for model evaluation. The forecasting results from these three techniques are shown in Fig 2, as compared with the measured values. The mean absolute error (MAE), root mean squared error (RMSE), normalized root mean squared error (NRMSE) [23] and the coefficient of determination (R^2) are introduced to assess the forecasting performance and how well the model fits the real data. Table I summarizes the forecasting performance of these methods. It can be seen that MAPA-PCA model is overall superior to other statistical models, such as MLR and ARIMA, in terms of NRMSE and R^2 . Then, the solar irradiance forecasting results obtained by MAPA-PCA model are provided to estimate the solar power output of a solar PV array under arbitrary solar radiances by using the output characteristic calculation model of PV cell given in [27].

C. Algorithm implementation on BESS-HVAC

As shown in Fig. 1, the physical layer integrates i) the lower controllers of HVAC and BESS that generate the control signal to track desired power references, and ii) power converters, i.e., DC/AC converter or AC/AC converter, which is an interface between loads and the grid. The control strategy and electrical diagram of HVAC can be referred to [9]. Here, we briefly describe the lower controller for BESS, as shown in Fig 3. The BESS control strategy is a closed-loop system to generate the corresponding control signal for voltage source converter (VSC), in order to track the power reference provided by the surplus-based consensus algorithm. It is cascaded by a power controller, a current controller and a pulse generator. The power controller is utilized to implement active power P_i^* control. Specifically, P_i^* is controlled by adjusting d-axis current I_d^* , while the reactive power is controlled by adjusting q-axis current, which is not included for the clarity of the figure here. The deviation between P_i and measured power P_i^* generates an error signal which is controlled by a proportional-integral (PI) controller to produce the current reference I_d^* . The current controller is then utilized to mitigate the deviation between the

I_d^* and measured current I_d , where the voltage reference V_d^* is produced by using a PI controller. The pulse generation module (PWM) is to transform the voltage reference in the d-q axis into the ABC-axis V_{abc}^* and a set of switch control signals (S_1, S_2, \dots) are generated by PWM technique to control VSC. The phase-lock loop (PLL) is to synchronize an output oscillator signal with the reference voltage V_{abc} . The phase angle signal ωt can be extracted for axis transformation. Meanwhile, each local node is required to send the local power information to control layer for state updates, as modelled in (21).

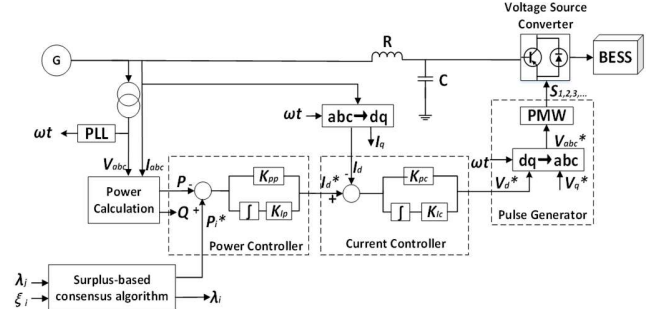


Fig 3. Control strategy of BESS.

The control layer of MAS framework conducts the surplus-based consensus algorithm, including state estimation, observation, and information exchange. The system identification block updates the agent’s $\lambda_i(k)$ and $\xi_i(k)$, described as beliefs in the Fig. 1. This block is the key to developing an energy management system based on the neighbours’ negotiation and network power information, as stated in (19) and (21). The agent’s desires indicate the objective function and local constraints ($\underline{P}_i, \bar{P}_i$). The agent’s intension is to provide power reference $P_i(k)$ for the lower controller of the HVAC or BESS. This upper controller calculates power reference following (20), by taking into account the state information, local constraints and global objectives from system identification block and neighbour negotiation block.

IV. CASE STUDIES AND RESULTS

An IEEE 14-bus system is utilized to carry out the studies, with 5 BESSs and 9 HVACs being distributed on local buses, as shown in Fig 4. The case studies are conducted under a globally coupled communication network, which is a strongly connected digraph. The parameters of HVACs and BESSs and their initial condition of each agent are given in Table II and Table III, respectively, from experiments presented in [28], and real weather data from UK Met office and a local weather station are used to establish solar power forecast as presented in Section III (B). These would make the theoretical model closer to the actual situation in the case studies. The initial value of power mismatch ξ_i on each local bus is set to zero. In most cases, we set the feedback gain to 0.07, if not specified otherwise.

A. Case study 1. Feasibility

1) Convergence effect

Convergence performance is shown in Fig 5 to illustrate the

effectiveness of the proposed algorithm. The total power mismatch P_d is set to 965 kW. Fig 5(a) shows the incremental cost curve, implying that all agents are able to achieve a common point at $\lambda^* = 5.6734$, which is equivalent to an optimal point calculated by (18). Fig 5(b) shows the power dispatch curve of the agents, where the HVACs and BESSs are operating at different power ratings within their own power boundaries. All local power mismatch ξ_i , $\forall i = 1, 2, \dots, n$ approach eventually to zero, as evidenced by Fig 5 (c). We omit the legend of agent in Fig 5(a) and (c) for simplification of the plots, if not specified otherwise.

We also compare the result with the algorithm in [19], as shown in Fig 5(d) as an example of a dynamic test. Assume that the total power generation changes from 965 kW to 985 kW at the 40th iteration and other settings remain the same. The algorithm in [19] shows a poor dynamic behaviour with the offset being 10 kW. This demonstrates that the proposed surplus-based distributed algorithm is superior in handling power changes with a quicker response and without steady-state error.

2) Performance of feedback gain ϵ

The initial ϵ is set to be $\epsilon = 0.0001$ and $\Delta\epsilon = 1 \times 10^{-4}$. As can be observed from Fig 6(a), with an increase of ϵ , the iterations for convergence decrease at the beginning and then increase. If ϵ is too large, the algorithm will go divergence and therefore there exists an optimal feedback gain, which is $\epsilon^* = 0.07$. Further study is made on the relationship between ϵ and

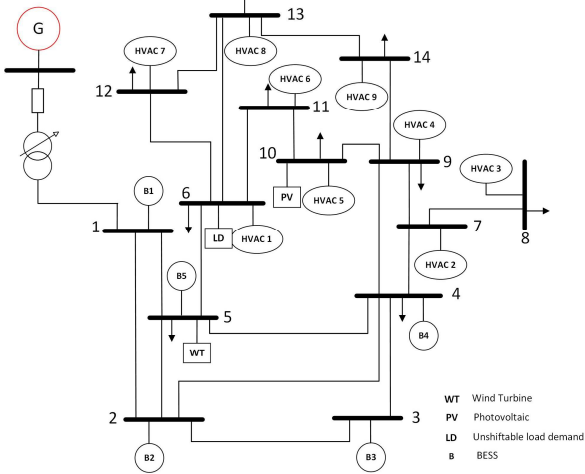


Fig 4. IEEE 14-bus system with 9 HVACs, 5 BESSs, 1 solar PV, 1 wind turbine and 1 unshiftable load.

TABLE II. COEFFICIENTS OF HVAC

No.	α_i	ω_i	$P_i(kW)$	$\bar{P}_i(kW)$	$P_i(0)$	$\lambda_i(0)$
1	0.1041	10.03	30	123.98	70	4.54
2	0.087	8.45	80	109.55	85	6.34
3	0.1564	19.16	80	137.93	85	7.43
4	0.095	15.63	50	120.19	100	3.37
5	0.097	14.97	103	176.19	120	8.31
6	0.1026	15.83	67	147.26	90	2.638
7	0.1345	19.45	20	110.43	80	2.207
8	0.0984	15.38	40	159.13	90	2.337
9	0.0924	18.05	43	123.98	120	4.126

TABLE III. COEFFICIENTS OF BESS

No.	a_i	b_i	$P_i(kW)$	$\bar{P}_i(kW)$	$P_i(0)$	$\lambda_i(0)$
1	0.2037	1.046	0	60	20	7.102
2	0.2815	1.2309	0	65	30	15.692
3	0.1987	1.0292	0	68	20	6.92
4	0.2092	1.1245	0	62	25	9.34
5	0.2247	1.0996	0	70	30	12.382

power mismatch in terms of the steady-state error, as shown in Fig 6(b). There are also optimal values of ϵ ranging from 0.6 to 1.0, during which steady state error of the system becomes minimal. Furthermore, we compare the result with the performance produced from a random strongly connected topology. By comparing Fig 6 and Fig 7, the directed network with more edges allows a wider range of ϵ to ensure the system stability while presenting less convergence time.

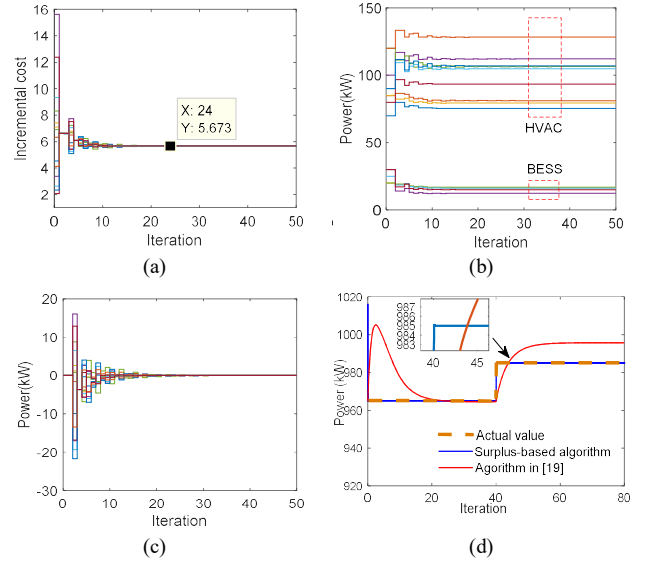


Fig 5. Convergence of (a) the incremental cost λ , (b) the power consumption P , (c) the local power mismatch ξ under the surplus-based consensus algorithm, and (d) comparison of the proposed algorithm with method in [19].

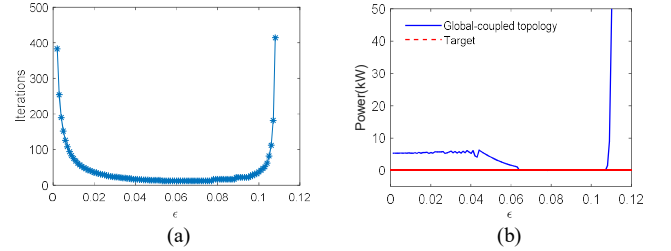


Fig 6. The effect of feedback gain ϵ on convergence under a global-coupled topology: (a) convergence time vs ϵ and (b) global power mismatch vs ϵ

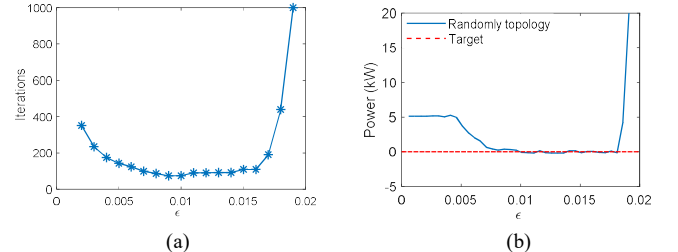


Fig 7. The effect of feedback gain ϵ on convergence under a randomly topology: (a) convergence time vs ϵ and (b) global power mismatch vs ϵ

B. Case study 2. Performance on communication networks

Studies are also conducted to evaluate the algorithm convergence under different directed communication

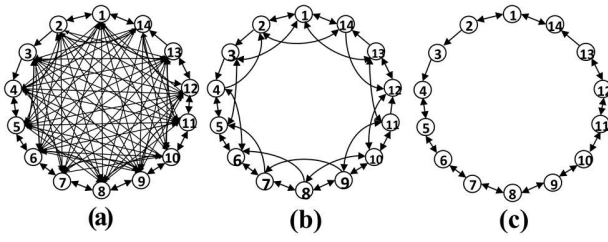


Fig 8. Three directed topology structures: (a) global coupled (b) NN coupled and (c) ring.

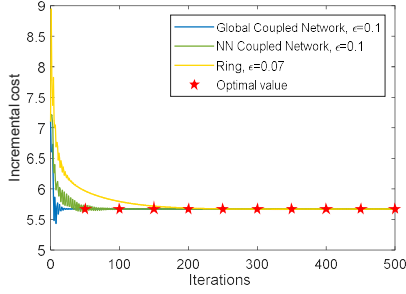


Fig 9. Convergence performance under different directed topologies.

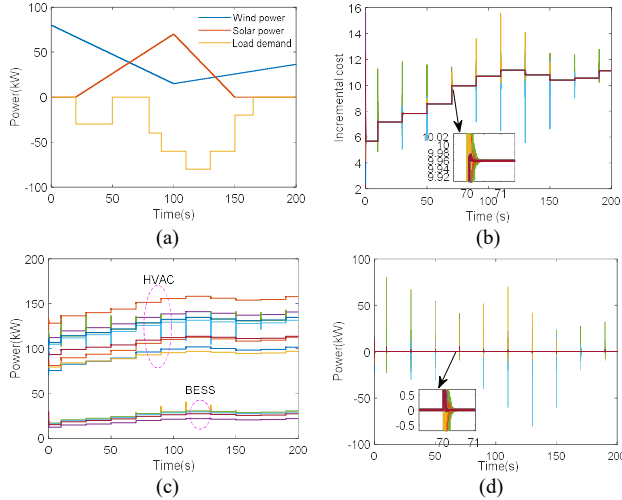


Fig 10. Energy dispatch scheme for HVAC-BESS under dynamic generation/demand: (a) The power profile of renewable generators and load demand; (b) Incremental cost; (c) Power reference provided to the HVACs and BESSs, and (d) Local power mismatch.

topologies. Three topology configurations are investigated, as shown in Fig 8, including globally coupled, nearest-neighbour coupled (NN-coupled) and ring networks. It can be observed in Fig 9 that these topologies have ability to achieve a consensus point with different convergence time. The globally coupled network, due to the best connectivity, only requires 30 iterations to converge and endures a large $\epsilon = 0.1$, while NN-coupled network requires 90 iterations to stabilize. In contrary, the ring network, due to poor connectivity, requires 200 iterations to converge and a relatively small $\epsilon = 0.07$. Consequently, the topology with a high density achieves the consensus with a fast speed whilst accommodating a larger upper bound of the feedback gain ϵ .

C. Case study 3. Energy dispatch on time-varying generation/demand

As depicted in Fig 4, a wind turbine, a solar PV and a unshiftable load are included, which are connected at bus 5, bus

10 and bus 6, respectively. The power profiles of the wind turbine, the solar PV and the load are given in Fig 10(a). The curves are given here based on the assumption that solar power is at a peak, wind power is at a valley and loads presents stochastic changes. The unshiftable load and distributed generators are integrated into system at 10 s and their power information is updated every 20s, where ($T_d = 20$ s) in this case. During each T_d , each agent calculates and then updates new state following (19)-(21), by receiving local power information from neighbouring agents.

Fig 10(b) shows that the incremental costs of all agents achieve a consensus promptly within T_d , thus ensuring HVAC and BESS performance is maximized. Fig 10(c) and Fig 10(d) present power references provided to each agent and power mismatch at the local buses, respectively. The local power mismatches all converge to zero during each T_d . Therefore, the total power consumption of BESSs and HVACs can compensate the global power mismatch.

D. Case study 4. Energy dispatch under solar power forecasts

This case focuses on developing a pre-scheduled energy dispatch scheme for the HVAC-BESS system under 24-h solar power forecasts in both summer and winter days, as shown in Fig 11(a)(b) and (c)(d), respectively. Take the summer day as an example, the blue line in Fig 11(a) represents a total power imbalance, consisting of initial power deviation $P_d = 965 \text{ kW}$ and 24-hour solar power generation, while the red line indicates that the HVAC-BESS can function to compensate the power imbalance. The pre-scheduled power references provided to HVACs and BESSs for energy dispatch are shown in Fig 11(b). Practically, power references will be broadcasted to the lower controller of HVACs and BESSs as a control signal to adjust their power consumption in order to follow the desired power output, as can be seen in Fig 3 as the example. The summer day represents there is more solar power generated while the winter day represents there is less solar power generated. The results demonstrated that the power balance can be met by combined operation of HVACs and BESSs for these days for different possible purposes, e.g., cooling in the summer days and heating in the winter days.

E. Case study 5. Plug-and-play functionality

One of the most significant features for a microgrid is its plug-and-play ability. In this case, we considered the network with 13 HVACs or BESSs that have already operated at optimal states before plugging the 1st HVAC at the 40th iteration. The initial conditions of units are the same as in Case study 1. The demand for HVAC 1 is set to $P_1 = 76 \text{ kW}$, $\xi_1 = -76 \text{ kW}$. From results in Fig 12(a) and (b), we can observe that the local power mismatch goes to zero after a short oscillation. The other units reduce their consumption for the sake of accommodating demand from the 1st HVAC. The incremental cost drops due to the lower average consumption; however, it eventually converges to an optimal value.

F. Case study 6. Scalability test

Scalability test is also performed for a large-scale power system to demonstrate robustness of the proposed approach. The key point is to render the algorithm to converge in a timely manner. This case is conducted under IEEE 57-bus system shown in [29], with 41 HVACs and 16 BESSs connected to buses, respectively. The case parameters refers to [28] and total power supply is set to 3845 kW. The communication network used is a strongly connected directed graph. Thus, the associated stochastic matrix can be determined by (1). The result in Fig 13 shows that output power of each HVAC and BESS converges to an optimal value and power balance can be maintained.

V. CONCLUSIONS

The growing capacity of renewable generators with uncertain generation patterns results in the need for increased system flexibility. The HVAC with a “slack” characteristic in nature in terms of running time and power output is a promising solution to engage the grid service. This paper proposed energy management framework with a surplus-based distributed algorithm for HVAC and BESS, to manage the variability of

renewable resources and address active power balance problem in the microgrid. The proposed distributed algorithm can solve the consensus problem under directed network, which relaxes the topology conditions. A 24-h energy dispatch scheme for HVAC and BESS is developed by incorporating predictions of solar power generation. The proposed framework is demonstrated to be feasible, scalable and therefore robust by the case studies. The work has not yet considered the voltage deviation and frequency response of the electrical network, and full physical dynamics of HVAC such as environmental temperature conditions and BESS such as both charging and discharging modes and capacity limitations. These will be investigated in future work.

APPENDIX

In this appendix, we demonstrate the proof of Theorem 1. We

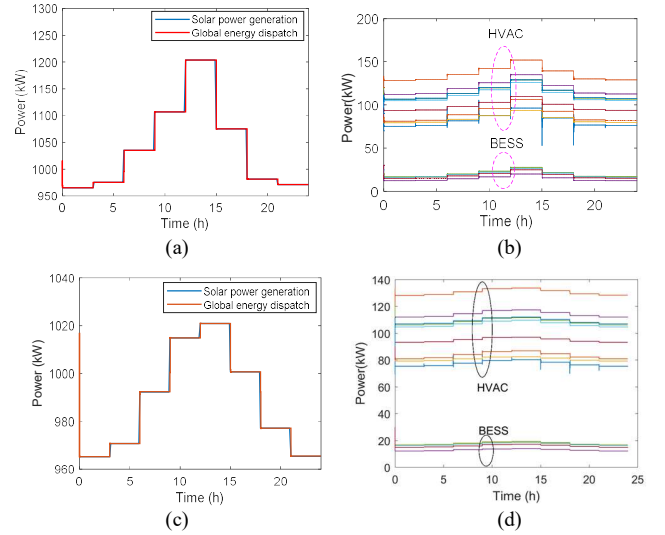


Fig 11. Energy dispatch scheme for HVAC-BESS under 24-hour solar power forecasts in summer and winter day: (a) (b) Power balance and Power references to HVACs and BESSs in a summer day; (c) (d) Power balance and power references to HVACs and BESSs in a winter day.

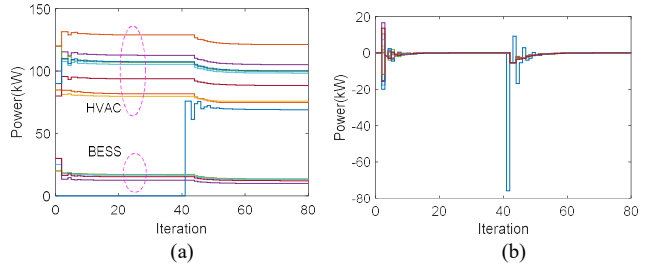


Fig 12. Response of HVAC-BESS under plug-and-play test: (a) Power references of HVACs and BESSs and (b) Local power mismatch.

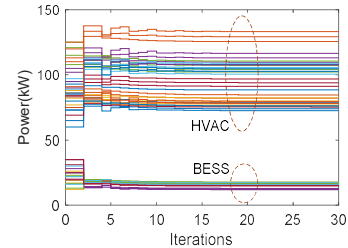


Fig 13. Power reference of HVACs and BESSs under IEEE 57-bus system.

firstly present relevant technical Lemmas and then the convergence analysis based on Lyapunov stability argument.

Lemma 1: The summation of $P_i(k) + \xi_i(k)$ for all agents following (19)-(21) is time-invariant at each $k \geq 0$, such that

$$\sum_{i=1}^n \xi_i(k) + \sum_{i=1}^n P_i(k) = P_d \quad (22)$$

Proof of Lemma 1: By summing all nodes in (21) and referring to the properties of matrix D , we obtain

$$\begin{aligned} \sum_{i=1}^n (\xi_i(k+1) + P_i(k+1)) &= \sum_{i=1}^n \left(\sum_{j \in \mathcal{N}_i^+} q_{ji} \xi_j(k) + P_i(k) \right) \\ \Rightarrow \sum_{i=1}^n \xi_i(k) + \sum_{i=1}^n P_i(k) &= \dots = \sum_{i=1}^n \xi_i(0) + \sum_{i=1}^n P_i(0) \end{aligned}$$

Suppose that $\xi_i(0) = 0$, for $i = 1, 2, \dots, n$, based on (10), we have:

$$\sum_{i=1}^n \xi_i(k) + \sum_{i=1}^n P_i(k) = P_d$$

Let us define the minimum and maximum state of λ_i at iteration k as below.

$$\underline{\lambda}(k) = \min_{i=1,2,\dots,n} \{\lambda_i(k)\} \text{ and } \bar{\lambda}(k) = \max_{i=1,2,\dots,n} \{\lambda_i(k)\} \quad (23)$$

The second lemma shows that the surplus vector of each agent ξ_i is upper bounded.

Lemma 2: Under the Algorithm 1, the following properties with respect to $\xi_i(k)$ hold.

- 1) If $\xi_i(0) \geq 0$, the power surplus $\xi_i(k)$ is non-negative for $i = 1, 2, \dots, n$ and $k \geq 1$.
- 2) If the time-invariant communication network \mathcal{G} is strongly connected, the power surplus $\xi_i(k)$ satisfies the following inequality

$$\xi_i(k) \leq \frac{\underline{\lambda}(k+2) - \underline{\lambda}(k+1)}{\varrho_e \varrho_q}$$

Proof of Lemma 2 (1). By considering (19), we have

$$\lambda_i(k+1) \leq \lambda_i(k) + \epsilon_i \xi_i(k)$$

Here, we distinguish two cases [22].

Case 1: $\lambda_i(k+1) \geq \lambda_i(k) \Rightarrow P_i(k+1) \geq P_i(k)$

Since $J_i(P_i)$ is a linear increasing function, so is $J_i^{-1}(\lambda_i)$. It is obtained that $\frac{dJ_i(P_i)}{dP_i} * \frac{dJ_i^{-1}(\lambda_i)}{d\lambda_i} = 1$. From **Error! Reference**

source not found. and (14), it can be derived $\frac{dJ_i(P_i)}{dP_i} \geq \varrho_i$.

Therefore, we have

$$\begin{aligned} P_i(k+1) - P_i(k) &\leq \frac{dJ_i^{-1}(\lambda_i)}{d\lambda_i} (\lambda_i(k+1) - \lambda_i(k)) \\ &\leq \frac{1}{\varrho_i} (\lambda_i(k+1) - \lambda_i(k)) \leq \frac{\epsilon_i \xi_i(k)}{\varrho_i} \end{aligned}$$

Then, by considering (19)-(21), it follows

$$\begin{aligned} \xi_i(k+1) &\geq q_i \xi_i(k) + \sum_{j \in \mathcal{N}_i^+, j \neq i} q_{ji} \xi_j(k) - \frac{\epsilon_i \xi_i(k)}{\varrho_i} \\ \xi_i(k+1) &\geq \left(q_i - \frac{\epsilon_i}{\varrho_i} \right) \xi_i(k) + \sum_{j \in \mathcal{N}_i^+, j \neq i} q_{ji} \xi_j(k) \end{aligned}$$

Case 2: $\lambda_i(k+1) < \lambda_i(k) \Rightarrow P_i(k+1) < P_i(k)$

From (19), it can be straightforward to obtain

$$\xi_i(k+1) \geq q_i \xi_i(k) + \sum_{j \in \mathcal{N}_i^+, j \neq i} q_{ji} \xi_j(k) \quad (24)$$

To summarize from above two cases, both $\left(q_i - \frac{\epsilon_i}{\varrho_i} \right)$ and $\sum_{j \in \mathcal{N}_i^+, j \neq i} q_{ji}$ are positive by (P1) and (P2). Suppose that $\xi_i(0) > 0$, for $i = 1, 2, \dots, n$, then, $\xi_i(k) \geq 0$ for $k \in \mathbb{Z}_+$

Proof of Lemma 2 (2). Firstly, we define a column vector $\xi = [\xi_1, \xi_2, \dots, \xi_n]^T$. An indicator matrix of $Q = \{q_{ij}\}$ can be defined by $S = \{s_{ij}\}$, where $s_{ij} = 1$, if $q_{ij} \neq 0$ while $s_{ij} = 0$ if $d_{ij} = 0$. It is straightforward to obtain by (24)

$$\xi(k+1) \geq \varrho_q (I + S) \xi(k)$$

where I is an identity matrix. By using the iterative product, for any $k \geq 0$, we obtain

$$\xi(k+1) \geq \varrho_q^{k+1} (I + S)^{k+1} \xi(0)$$

The Corollary 6.2.19 in [30] proves that if and only if \mathcal{G} is strongly connected, the following inequality is true.

$$(I + S)^{k+1} = I + (k+1)S + \dots + S^{k+1} > 0$$

Therefore,

$$\xi(k+1) \geq \varrho_q^{k+1} \xi(0)$$

For the entry in vector ξ , it can be derived

$$\xi_i(k+1) \geq \varrho_q \xi_i(k) \quad \text{for } i = 1, 2, \dots, n \quad (25)$$

Suppose that $\lambda_m(k+1) = \underline{\lambda}(k+1)$ when $i = m$. In (19), note that the first two term is a convex combination of $\lambda_i(k)$ and $\lambda_j(k)$, where $j \in \mathcal{N}_i$ and $c_i(k) = 1$. We therefore have [22]

$$\lambda_i(k) + \sum_{j \in \mathcal{N}_i} p_{ij} (\lambda_j(k) - \lambda_i(k)) \geq \min_{j \in \{i\} \cup \mathcal{N}_i} \{\lambda_j(k)\} = \underline{\lambda}(k)$$

Substituting the above into (19), the following equality holds.

$$\lambda_i(k+1) \geq \underline{\lambda}(k) + \epsilon_i \xi_i(k) \geq \underline{\lambda}(k) + \varrho_e \xi_i(k)$$

Replacing i with m , k with $k+1$, we obtain

$$\xi_i(k+1) \leq \frac{\underline{\lambda}(k+2) - \underline{\lambda}(k+1)}{\varrho_e} \quad (26)$$

Plugging (26) into (25),

$$\xi_i(k) \leq \frac{\underline{\lambda}(k+2) - \underline{\lambda}(k+1)}{\varrho_e \varrho_q}$$

The third lemma presents the properties with respect to $\underline{\lambda}(k)$ and equilibrium point of the algorithm.

Lemma 3: Under the Algorithm 1, the following holds.

- 1) The minimum state $\underline{\lambda}(k)$ is non-decreasing for every k , that is $\underline{\lambda}(k_1) \leq \underline{\lambda}(k_2)$, if $k_1 < k_2$.
- 2) There is a scalar λ_0 that satisfies $\underline{\lambda}(k) \leq \lambda_0$ for $k \in \mathbb{Z}_+$. If $\underline{\lambda}(k) = \bar{\lambda}(k) = \lambda_0$, then $\lambda_i(k) = \lambda_0$ and $\xi_i(k) = 0$, for $i = 1, 2, \dots, n$. The consensus is thus achieved.

Proof of Lemma 3 (1). From Lemma 2, we obtain that

$$\underline{\lambda}(k+1) \geq \underline{\lambda}(k)$$

where $\underline{\lambda}(k)$ is non-decreasing for all $k \in \mathbb{Z}_+$.

Proof of Lemma 3 (2). Suppose on the contrary that $\underline{\lambda}(k) > \lambda_0$ for $k \in \mathbb{Z}_+$. Under the non-decreasing properties of $\underline{\lambda}(k)$, if we define $J_i(\bar{P}_i) = \underline{\lambda}(k)$, there exists a k' ($k' > k$), satisfying,

$$\underline{\lambda}(k') > \lambda_0 > \underline{\lambda}(k)$$

Correspondingly, $P_i(k') > \bar{P}_i$ for all $i = 1, 2, \dots, n$. Therefore:

$$\sum_{i=1}^n P_i(k') > P_d$$

If (22) is held for $k = k'$, the only possible case is $\sum_{i=1}^n \xi_i(k') < 0$. However, this conflicts with Lemma 2. Thus, the minimum state of λ_i holds $\underline{\lambda}(k) \leq \lambda_0$.

Provided that $\underline{\lambda}(k) = \lambda_0$, the same argument holds that $\bar{\lambda}(k) = \lambda_0$. Thus, $\lambda_i(k) = \lambda_0$ and $\xi_i(k) = 0$, for all i and $k \rightarrow \infty$, the consensus of Algorithm 1 is achieved.

Given an initial condition $(\lambda_i(0), \xi_i(0) = 0)$, let Ω be a finite-dimensional Euclidean space with respect to the equilibrium solution $(\lambda_0, 0)$ of the discrete-time system (19)-(21). The equality constraint in Lemma 1 holds.

$$\Omega(\lambda_0, 0) = \left\{ (\lambda, \xi) \in \mathbb{R}_{2n}, \lambda_0 = \Phi^{-1} \left(\frac{1_n \Phi(\lambda(0))}{n} \right), \xi \geq 0 \right\} \subset \mathbb{R}_{2n} \quad (27)$$

where $\lambda, \xi, \Phi(\lambda)$ denote the column vector of $\lambda_i, \xi_i, \Phi_i(\lambda_i)$ respectively, and 1_n is a column vector with all entries being one. Therefore, the space $\Omega(\lambda_0, 0)$ specifies a trajectory of (λ, ξ) converging to an equilibrium point $(\lambda_0 1_n, 0_n)$: $(\lambda, \xi) \in \Omega(\lambda_0, 0)$, whilst (λ, ξ) is updated with a discrete time system (19)-(21).

Lemma 4: (Theorem 3 in [31]) Consider a discrete map defined by the algorithm (19)-(21) satisfying $(\lambda, \xi) \in \Omega$, with the unique equilibrium point being $(\lambda_0 1_n, 0_n)$. Consider a continuous set-valued function $V'(\lambda_i(k), \xi_i(k))$ and a continuous function δ , satisfying:

- 1) V' is bounded on the bounded set of $\Omega(\lambda_0, 0)$. V' is positive definite with respect to an equilibrium point $(\lambda_0, 0)$, that is $V'(\Omega(\lambda_0, 0)) = 0$ and $\mu(V'(\lambda, \xi)) > 0$ for $(\lambda, \xi) \in \Omega(\lambda_0, 0) - (\lambda_0 1_n, 0_n)$.
- 2) δ is a positive definite function with respect to $(\lambda_0 1_n, 0_n)$ such that $\delta(\lambda_0, 0) = 0$ at the equilibrium point and $\delta(\lambda, \xi) > 0$ for $(\lambda, \xi) \in \Omega(\lambda_0, 0) - (\lambda_0 1_n, 0_n)$.
- 3) $V'(\lambda(k+1), \xi(k+1)) - V'(\lambda(k), \xi(k)) \leq -\delta(\lambda(k), \xi(k))$ for $\forall (\lambda, \xi) \in \Omega(\lambda_0, 0)$

If the $V'(\lambda, \xi)$ is bounded for all $(\lambda, \xi) \in \Omega(\lambda_0, 0)$ and the incremental of V' satisfies condition 3), then the algorithm (19)-(21) is asymptotically stable with respect to $(\lambda_0 1_n, 0_n)$.

The function δ characterizes the decrease of $\mu(V')$ for $(\lambda, \xi) \in \Omega(\lambda_0, 0)$. The set-valued function V' plays the role of a Lyapunov function, which is a non-increasing bounded function. The proof of Lemma 4 is demonstrated in [31].

Proof of Theorem 1: We now proceed to the proof of Theorem 1, based on Lyapunov stability theorem. Consider a Lyapunov function $V(\lambda, \xi)$, $(\lambda, \xi) \in \Omega(\lambda_0, 0)$, defined as:

$$V(\lambda, \xi) = \Phi^{-1} \left(\frac{1_n(\xi + \Phi(\lambda))}{n} \right) - \underline{\lambda} \quad (28)$$

Clearly, the function V is continuous on (λ, ξ) . According to the properties of $\underline{\lambda}$ in Lemma 3, we obtain that V is bounded on the subset of $\Omega(\lambda_0, 0)$ and non-increasing for $k \geq 0$. Furthermore, $V(\lambda, \xi) > 0$ if $(\lambda, \xi) \in \Omega(\lambda_0, 0) - (\lambda_0 1_n, 0_n)$

and $V(\lambda, \xi) = 0$ if $(\lambda, \xi) \rightarrow (\lambda_0 1_n, 0_n)$.

Then, an ancillary positive function δ is given by:

$$\delta(\lambda, \xi) = \inf V(\lambda(k), \xi(k)) - V(\lambda(k+1), \xi(k+1)) \quad (29)$$

Since $V(\lambda, \xi)$ is a non-increasing function, $\delta(\lambda, \xi)$ is positive definite when $(\lambda, \xi) \in \Omega(\lambda_0, 0) - (\lambda_0 1_n, 0_n)$. $\delta(\lambda, \xi) = 0$ at the equilibrium point $(\lambda_0 1_n, 0_n)$. \inf denotes infimum. The function V and δ defined in (28) and (29) satisfies the conditions in Lemma 4, which implies that the dynamic system becomes asymptotically consensus stable at the point $(\lambda_0 1_n, 0_n)$.

REFERENCES

- [1] D. T. Vedullapalli, S. Member, R. Hadidi, and B. Schroeder, "Combined HVAC and Battery Scheduling for Demand Response in a Building," *IEEE Trans. Ind. Appl.*, vol. 55, no. 6, pp. 7008–7014, 2019.
- [2] B. P. Rasmussen and A. G. Alleyne, "Dynamic Modeling and Advanced Control of Air Conditioning and Refrigeration Systems," University of Illinois at Urbana-Champaign Air, 2006.
- [3] A. Aswani, N. Master, J. Taneja, D. Culler, and C. Tomlin, "Reducing Transient and Steady State Electricity Consumption in HVAC Using Learning-Based Model-Predictive Control," *Proc. IEEE*, vol. 100, no. 1, pp. 240–253, 2012.
- [4] E. Rezaei, S. Member, and H. Dagdougui, "Optimal Real-Time Energy Management in Apartment Building Integrating Microgrid With Multizone HVAC Control," *IEEE Trans. Ind. Informatics*, vol. 16, no. 11, pp. 6848–6856, 2020.
- [5] N. Mahdavi, J. H. Braslavsky, S. Member, M. M. Seron, and S. R. West, "Model predictive control of distributed air-conditioning loads to compensate fluctuations in solar power," *IEEE Trans. Smart Grid*, vol. 8, no. 6, pp. 3055–3065, 2017.
- [6] K. Ma, G. Hu, and C. J. Spanos, "Energy Management Considering Load Operations and Forecast Errors With Application to HVAC Systems," *IEEE Trans. Smart Grid*, vol. 9, no. 2, pp. 605–614, 2018.
- [7] Y. Li, D. W. Gao, and S. Member, "A Distributed Double-Newton Descent Algorithm for Cooperative Energy Management of Multiple Energy Bodies in Energy Internet," *IEEE Trans. Ind. Informatics*, vol. 17, no. 9, pp. 5993–6003, 2021.
- [8] Y. Li, D. W. Gao, W. Gao, H. Zhang, and J. Zhou, "Double-Mode Energy Management for Multi-Energy System via Distributed Dynamic," *IEEE Trans. Smart Grid*, vol. 11, no. 6, pp. 5339–5356, 2020.
- [9] J. Ma, X. Ma, and S. Ilic, "HVAC-Based Cooperative Algorithms for Demand Side Management in a Microgrid," *Energies*, vol. 12, no. 22, p. 4276, 2019.
- [10] J. Choi, I. Choi, and G. Ahn, "Advanced Power Sharing Method to Improve the Energy Efficiency of Multiple Battery Energy Storages System," *IEEE Trans. Smart Grid*, vol. 9, no. 2, pp. 1292–1300, 2018.
- [11] J. Hu and A. Lanzon, "Distributed Finite-Time Consensus Control for Heterogeneous Battery Energy Storage Systems in Droop-Controlled Microgrids," *IEEE Trans. Smart Grid*, vol. 10, no. 5, pp. 4751–4761, 2019.
- [12] Y. Wang *et al.*, "Aggregated Energy Storage for Power System Frequency Control: A Finite-Time Consensus Approach," *IEEE Trans. Smart Grid*, vol. 10, no. 4, pp. 3675–3686, 2019.
- [13] N. Rahbari-asr, S. Member, and M. Chow, "Cooperative Distributed Demand Management for Community Charging of PHEV / PEVs Based on KKT Conditions and Consensus Networks," *IEEE Trans. Ind. Informatics*, vol. 10, no. 3, pp. 1907–1916, 2014.
- [14] K. Rahbar and C. C. Chai, "Optimization of Battery Energy Storage and Building HVAC Systems for Energy Cost Efficiency and Frequency Regulation," in *IEEE Power & Energy Society Innovative Smart Grid Technologies Conference (ISGT)*, 2020, pp. 0–4.
- [15] T. Wei *et al.*, "Battery Management and Application for Energy-Efficient Buildings," in *51st ACM/EDAC/IEEE Design Automation Conference (DAC)*, 2014.
- [16] Y. Xu, W. Zhang, G. Hug, S. Kar, and Z. Li, "Cooperative Control of Distributed Energy Storage Systems in a Microgrid," *IEEE Trans. Smart Grid*, vol. 6, no. 1, pp. 238–248, 2015.
- [17] L. An, J. Duan, M.-Y. Chow, and A. Duel-Hallen, "A Distributed and Resilient Bargaining Game for Energy Cooperation," *IEEE Trans. Industrial Informatics*, vol. 15, no. 8, pp. 4721–4730, 2019.

- [18] R. Wang, B. Zhang, and L. Wang, "Distributed Consensus Based Algorithm for Economic Dispatch in a Microgrid," *IEEE Trans. Smart Grid*, vol. in press, 2019.
- [19] T. Zhao and Z. Ding, "Cooperative Optimal Control of Battery Energy Storage System under Wind Uncertainties in a Microgrid," *IEEE Trans. Power Syst.*, vol. 33, no. 2, pp. 2292–2300, 2018.
- [20] N. Rahbari-asr, S. Member, U. Ojha, S. Member, and Z. Zhang, "Incremental Welfare Consensus Algorithm for Cooperative Distributed Generation / Demand Response in Smart Grid," *IEEE Trans. Smart Grid*, vol. 5, no. 6, pp. 2836–2845, 2014.
- [21] Y. Zhu, D. Zhao, and S. Member, "Control-Limited Adaptive Dynamic Programming for Multi-Battery Energy Storage Systems," *IEEE Trans. Smart Grid*, vol. 10, no. 4, pp. 4235–4244, 2019.
- [22] Y. Xu *et al.*, "A Distributed Algorithm for Resource Allocation Over Dynamic Digraphs," *IEEE Trans. signal Process.*, vol. 65, no. 10, pp. 2600–2612, 2017.
- [23] J. Ma and X. Ma, "State-of-the-art forecasting algorithms for microgrids," in *23rd IEEE International Conference on Automation and Computing*, 2017, no. September, pp. 7–8.
- [24] J. Ma and X. Ma, "Consensus-based Hierarchical Demand Side Management in Microgrid," in *25th International Conference on Automation & Computing*, 2019, no. September, pp. 5–7.
- [25] Y. Wang, Y. Shen, S. Mao, S. Member, G. Cao, and R. M. Nelms, "Adaptive Learning Hybrid Model for Solar Intensity Forecasting," *IEEE Trans. Ind. Informatics*, vol. 14, no. 4, pp. 1635–1645, 2018.
- [26] J. Ma and X. Ma, "A review of forecasting algorithms and energy management strategies for microgrids," *Syst. Sci. Control Eng.*, vol. 6, no. 1, pp. 237–248, 2018.
- [27] J. Ma and X. Ma, "Distributed Control of Battery Energy Storage System in a Microgrid.pdf," in *8th International Conference on Renewable Energy Research and Applications*, 2019.
- [28] C. Zhao, J. He, P. Cheng, and J. Chen, "Consensus-Based Energy Management in Smart Grid With Transmission Losses and Directed Communication," *IEEE Trans. Smart Grid*, vol. 8, no. 5, pp. 2049–2061, 2017.
- [29] Power systems test case archive, "IEEE 57-bus system." [Online]. Available: <http://labs.ece.uw.edu/pstca/pf57/ieee57cdf.txt>.
- [30] R. . Horn and C. . Johnson, *Matrix Analysis*. Cambridge UK: Cambridge University Press, 1985.
- [31] L. Moreau, "Stability of Multiagent Systems With Time-Dependent," *IEEE Trans. Automat. Contr.*, vol. 50, no. 2, pp. 169–182, 2005.